Original Manuscript

Journal of Vibration and Control
2022, Vol. 0(0) 1–11

DOI: 10.1177/10775463221077490
journals.sagepub.com/home/jvc
SAGE

Proper location of the transducers for an active noise barrier

Shahin Sohrabi[1], Teresa Pàmies Gómez[1], and Jordi Romeu Garbí[1]

Abstract

The main intention of this study is to propose general criteria for the locations of the control sources and error microphones that improve the performance of the active noise barrier. Based on the proposed criteria of this study, the greater reduction is attained when the diffracted field of the noise source is canceled with the diffracted field of the control sources, that is, it is suggested to locate the control sources on the incident side and below the path that connects the furthest point in the shadow zone to the edge of the barrier. Furthermore, it is suggested that the error microphones are most suitably placed on the shadow side of the barrier where they are under the diffracted field of both the primary and control sources. The results also show that with these general criteria, the active noise control achieves an extra reduction that varies from 14.9 to 3.9 dB (for the third-octave band from 63 Hz to 1 kHz) and 9.3 dB for the broadband noises.

Keywords

active noise barrier, location of sources, location of error microphones, narrowband and broadband spectra, noise attenuation

1. Introduction

The use of active control systems to reduce undesired propagated noise and vibration is a fairly widespread solution (Aggogeri et al., 2020; Aslan and Paurobally, 2018), especially for low-frequency disturbances. During the past two decades, this technique was investigated in several studies to improve the performance of noise barriers (Borchi et al., 2016; Huang et al., 2015; Lee et al., 2019). The efficiency of an active noise barrier (ANB) depends on the number and location of transducers. The performance of the active noise barriers is measured by the extra attenuation achieved at the shadow zone, and it is shown that the best performance is obtained when error microphones are deployed within the shadow zone (Berkhoff, 2005). However, deploying error microphones in this area can require considerable hardware and interferes with the ongoing activities (Huang et al., 2015; Wang et al., 2016). Moreover, great outdoor distances between control sources and the receivers can lead to a degradation in the coherence of the error and reference signals, causing a loss in performance (Ai et al., 2000). Therefore, it is preferable to pursue a configuration with transducers close to the barrier.

Omoto et al. (Omoto et al., 1997) placed the error microphones on the barrier edge, and the secondary sources were located on the same side as the primary source, but with different angles and radii from the top edge. Their results revealed that the distance between error microphones should be less than half of the wavelength to achieve a noticeable attenuation. Guo et al. (Guo et al., 1997) studied a similar configuration and concluded that the optimal distance between secondary sources and error microphones depends on the distance between error microphones and the frequency.

The diffracted wave can also be tentatively canceled when secondary sources instead of error microphones are placed on the edge of the barrier. Niu et al. (Niu et al., 2007) placed the secondary sources on the top of the edge instead and explored the efficiency of the active noise barrier for only three different arrangements of error microphones near the edge. Their observations showed that better results are achieved when the error microphones were placed above the secondary sources and that attenuation depends on the distance between control sources and error microphones.

[1]Department of Acoustic and Mechanical Engineering Laboratory (LEAM), Technical University of Catalonia (UPC), Terrassa, Spain

Received: 21 June 2021; accepted: 14 January 2022

Corresponding author:
Shahin Sohrabi, Department of Acoustic and Mechanical Engineering Laboratory (LEAM), Technical University of Catalonia (UPC), Colom street, N 11, Terrassa 08222, Spain.
Email: shahin.sohrabi@upc.edu

Other investigations seek configurations of transducers placed not on the edge of the barrier but near it. Han et al. (Han and Qiu, 2007) placed three secondary sources at the bottom of the incident side of the barrier and three error microphones at three different positions close to the edge, getting a similar performance for all three positions as a result.

Other studies consider the secondary sources in the receiver zone (Duhamel et al., 1998; Wang et al., 2016) or include the secondary sources and error microphones vertically along the receiver side of the barrier (Nagamatsu et al., 2000). Giving these configurations, generally poor results achieved, although only one position was tested in each case.

More recently, a development by the authors (Sohrabi et al., 2020), applying a two-step optimization procedure for the location of both sets of transducers close to the barrier for a typical construction environment, showed that there is a different suitable configuration of the microphones which gives a similar cancellation at the receiver zone far from the barrier.

The prior studies investigated very limited configurations of control sources and error microphones placed "on" or "close" the top edge of the barrier. As a result, neither an optimal design nor a general rule for a practical design of an active noise barrier has been established. The main objective of the present study is to define general criteria for the placements of the control units close to an active noise barrier for both narrowband and broadband noise. Also, the cancellation mechanism of the proposed configurations is analyzed.

2. Theory

2.1. Diffraction model

In this study, the pressure of diffracted field (P_D) is calculated by MacDonald's solution described in equation (1), (Li and Wong, 2005).

$$P_D = \frac{k^2 \rho\, c}{4\pi} q_0 \left[\operatorname{sgn}(\zeta_1) \int_{|\zeta_1|}^{\infty} \frac{H_1^{(1)}(kR_1 + s^2)}{\sqrt{s^2 + 2kR_1}}\, ds + \operatorname{sgn}(\zeta_2) \int_{|\zeta_2|}^{\infty} \frac{H_1^{(1)}(kR_2 + s^2)}{\sqrt{s^2 + 2kR_2}}\, ds \right] \tag{1}$$

where k (m^{-1}) is the acoustic wavenumber, q_0 ($m^3.s^{-1}$) is the source strength, and ρ ($kg.m^{-3}$) and c ($m.s^{-1}$) are the air density and speed of sound in air, respectively. $H_1^{(1)}(\,)$ is the Hankel function of the first kind, R_1 and R_2 are the distances (in meters) from the source and its barrier image to the receiver, respectively, illustrated in Figure 1. s is the variable of the contour integral, and the limits of the two contour integrals in equation (1) are determined according to

$$\zeta_1 = \operatorname{sgn}(|\theta_s - \theta_r| - \pi)\sqrt{k(R' - R_1)} \tag{2}$$

$$\zeta_2 = \operatorname{sgn}(\theta_s + \theta_r - \pi)\sqrt{k(R' - R_2)} \tag{3}$$

where sgn() is the sign function and θ_s θ_r are the source and receiver angles to the barrier's face, respectively. R' (m) is the shortest path from the source to the receiver through the edge and it equals to $R' = r_s + r_r$, shown in Figure 1(a). Direct and reflected pressures are calculated as follows, (Nelson et al., 1992)

$$P_d = \left(-\frac{ik\rho\, c}{4\pi} q_0\right) \frac{e^{ikR_1}}{R_1} \tag{4}$$

$$P_r = \left(-\frac{ik\rho\, c}{4\pi} q_0\right) \frac{e^{ikR_2}}{R_2} \tag{5}$$

The effect of the soil's reflection is considered based on the image method (Matsui et al., 1989). Thus, the total pressure ($\boldsymbol{P_T}$) at a receiver is the superposition of all wave paths from the source to the receiver. For a receiver in the shadow zone, $\boldsymbol{P_T} = \boldsymbol{P_1} + Q_r\boldsymbol{P_2} + Q_s\boldsymbol{P_3} + Q_rQ_s\boldsymbol{P_4}$, where $\boldsymbol{P_1}$ is the diffracted pressure and $\boldsymbol{P_2}$ to $\boldsymbol{P_4}$ are the diffracted sound waves that are reflected from the soil on both sides of the barrier (Figure 1(b)). In this equation, Q_s and Q_r are the spherical wave reflections at the source and receiver sides, respectively, and depend on the acoustical characteristic of the ground and the source/receiver geometry (Attenborough, 1988; Embleton, 1996). In the present study, the suitable locations of the transducers are searched for totally absorbent ($Q_s = Q_r = 0$) and perfectly reflecting soils ($Q_s = Q_r = 1$).

2.2. Active noise control for barriers

The optimum configuration for an active noise barrier is when a set of error microphones are located in the target area and the active control system reduces the pressure in those points. However, for a practical design, the transducers should locate close to the barrier to avoid interference with the activities and also for the feasibility of the installation. In this study, the "barrier zone" (shown in Figure 1) is a region where transducers are intended to be deployed close to the barrier.

The procedures of finding the suitable locations for the transducers of an active noise barrier are followed by two steps (Palacios et al., 2010; Romeu et al., 2015; Sohrabi et al., 2020). The first step provides the proper position of the control sources that ensures the minimum acoustic pressure at the target zone. The second step finds the suitable position of the error microphones, while the

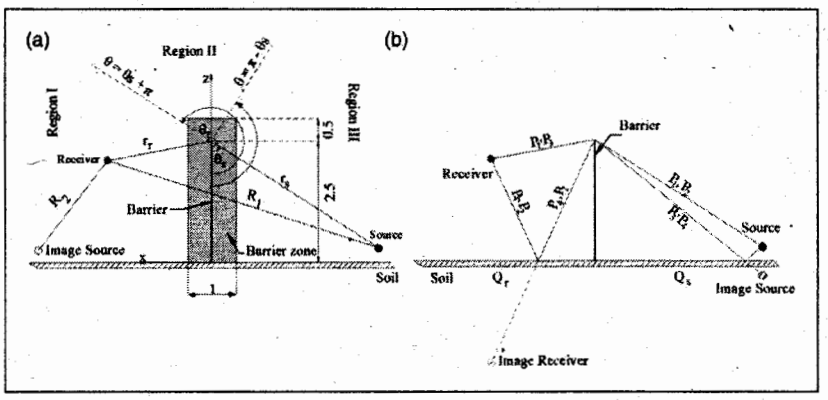

Figure 1. Schematic diagram of the barrier (a) with different regions around it and the barrier zone and (b) four diffracted pressures (P_1 to P_4) transmitted to an arbitrary receiver point from a noise source. (Units are in meters).

secondary sources are placed at the position of the previous step. It should be emphasized that the best position for error microphones in this study is the one that maximally reduces the acoustic pressure at the target zone, which is far from the location of the error microphones. The active noise barrier obtains the highest attenuation at the target zone with this configuration.

2.2.1. Location of the secondary sources. The sound pressure at a receiver is the superposition of a primary field and a secondary field, which is the contribution of secondary sources (Nelson et al., 1992; Qiu et al., 2017). Equation (6) describes the total pressure ($\boldsymbol{P}_r$) at the receivers in the target zone

$$\boldsymbol{P}_r = \boldsymbol{Z}_{Pr}q_P + \boldsymbol{Z}_{sr}\boldsymbol{q}_{sr} \tag{6}$$

where $\boldsymbol{Z}_{Pr}$ is the vector of complex impedances for the primary source with strength q_P at receiver points. $\boldsymbol{Z}_{sr}$ is an $M \times N$ impedance matrix, corresponding to N control source at M receiver points, and $\boldsymbol{q}_{sr}$ is the vector for secondary source strength. The total squared pressure at the receiver points is described as below

$$\begin{aligned} J_{pr} = \boldsymbol{P}_r^H\boldsymbol{P}_r = |q_p|^2\boldsymbol{Z}_{Pr}^{\mathrm{H}}\boldsymbol{Z}_{Pr} + q_p^*\boldsymbol{Z}_{Pr}^{\mathrm{H}}\boldsymbol{Z}_{sr}\boldsymbol{q}_{sr} \\ + \boldsymbol{q}_{sr}^{\mathrm{H}}\boldsymbol{Z}_{sr}^{\mathrm{H}}\boldsymbol{Z}_{pr}q_P + \boldsymbol{q}_{sr}^{\mathrm{H}}\boldsymbol{Z}_{sr}^{\mathrm{H}}\boldsymbol{Z}_{sr}\boldsymbol{q}_{sr} \end{aligned} \tag{7}$$

where the symbol H denotes the complex conjugate of the vector transpose. The unique minimum values for the control sources' strengths that minimize equation (7) and guarantee the maximum reduction at the receiver are specified by (Nelson et al., 1992)

$$\boldsymbol{q}_{sr} = -\left(\boldsymbol{Z}_{sr}^H\boldsymbol{Z}_{sr}\right)^{-1}\left(\boldsymbol{Z}_{sr}^H\boldsymbol{Z}_{pr}q_P\right) \tag{8}$$

In the present work, the efficiency of the active noise barrier at a tonal noise is calculated by the average insertion loss, $\overline{IL}_r$, and at the receiver points is defined by equation (9) (Nelson et al., 1992)

$$\overline{IL}_r = 10log_{10}\left(\frac{\sum_j^M\left|\boldsymbol{P}_j^{OFF}\right|^2}{\sum_j^M\left|\boldsymbol{P}_j^{ON}\right|^2}\right) \tag{9}$$

where $\boldsymbol{P}_j^{ON} = \boldsymbol{Z}_{Pr}q_P + \boldsymbol{Z}_{sr}\boldsymbol{q}_{sr}$ and $\boldsymbol{P}_j^{OFF} = \boldsymbol{Z}_{Pr}q_P$ are the pressure at jth receiver point when the control system is "*ON*" and "*OFF*", respectively. With the same concept as equation (9) is derived for a narrowband frequency, the overall insertion loss, IL_o achieved by the active noise control system for a broadband spectrum is computed by equation (10)

$$IL_o = 10\ log\left(\frac{\sum_{i=1}^{i=n}\sum_{j=1}^{M}\left|\boldsymbol{P}_{ij}^{OFF}\right|^2}{\sum_{i=1}^{i=n}\sum_{j=1}^{M}\left|\boldsymbol{P}_{ij}^{ON}\right|^2}\right) \tag{10}$$

where $\boldsymbol{P}_{ij}$ is the pressure of ith tonal noise at the jth receiver points. The best position for the secondary sources within the barrier zone is the one that gives the maximum $\overline{IL}_r$ or IL_o, depending on whether the noise is narrowband or broadband, respectively.

2.2.2. Location of the error microphones. The total sound pressure at the error microphone $\boldsymbol{P}_e$ is expressed by equation (11) (Nelson et al., 1992; Qiu et al., 2017)

$$\boldsymbol{P}_e = \boldsymbol{Z}_{Pe}q_P + \boldsymbol{Z}_{se}\boldsymbol{q}_{se} \tag{11}$$

where $\boldsymbol{Z}_{Pe}$, $\boldsymbol{Z}_{se}$, and $\boldsymbol{q}_{se}$ have the same definition as described in equation (6) but for the error microphones that are located in the barrier zone instead of the target zone. Equation (12) denotes the vector of the control sources' strength while the squared pressure is minimized at the error microphones.

$$\boldsymbol{q}_{se} = -\left(\boldsymbol{Z}_{se}^H\boldsymbol{Z}_{se}\right)^{-1}\left(\boldsymbol{Z}_{se}^H\boldsymbol{Z}_{pe}q_P\right) \tag{12}$$

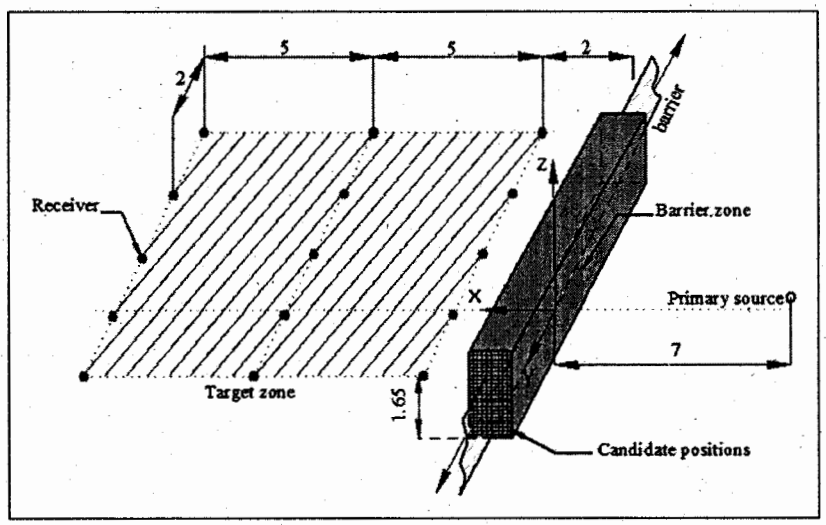

Figure 2. Schematic diagram of an infinite barrier with 15 receiver points in the shadow zone. The grid shows the candidate positions for the arrays of transducers. (Units are in meters).

Table 1. $\overline{IL}_r$ (dB) at the best positions of control sources, at different frequencies.

Absorbent soil				Hard soil		
Freq.(Hz)	(X_S, Z_S) m	$\overline{IL}_r$ (dB)	$\overline{IL}_{passive}$	(X_S, Z_S) m	$\overline{IL}_r$ (dB)	$\overline{IL}_{passive}$
63	(0.5, 2.3)	31.7	7.7	(−0.5, 1.0)	28.3	8.4
80	(−0.1, 0)	38.2	8.3	(0.1, 0.6)	34.1	9.4
100	(−0.2, 0.2)	34.5	8.9	(−0.1, 0)	29.1	8.9
125	(−0.3, 0.1)	33.2	9.6	(−0.5, 2.2)	28.4	8.4
160	(−0.5, 0.4)	33.5	10.4	(−0.5, 1.7)	26.2	9.8
200	(−0.4, 0)	37.3	11.1	(−0.5, 2.4)	22.4	15.2
250	(−0.5, 0)	32.1	11.9	(−0.5, 1.1)	23.6	12.1
315	(−0.5, 0)	26.2	12.7	(0.5, 2.2)	23.9	12.5
400	(−0.5, 0)	22.3	13.6	(−0.5, 2.5)	19.7	14.6
500	(−0.5, 2.7)	19.8	14.4	(−0.5, 2.2)	15.1	20.0
630	(−0.5, 0.9)	15.7	15.4	(−0.5, 0.2)	14.7	21.6
800	(−0.5, 0.5)	11.7	16.4	(−0.2, 2.7)	16.1	34.1
1000	(−0.5, 2.1)	11.7	17.4	(−0.5, 1.8)	10.6	24.1
Overall	(−0.5, 0)	(IL_o) 21.6	11.2	(−0.5, 1.8)	(IL_o) 21.3	11.4

The best position for the error microphones within the barrier zone is where the maximum $\overline{IL}_r$ (Equation (9)) or IL_o (Equation (10)) obtains at the target zone, but with $\boldsymbol{P}_j^{ON} = \boldsymbol{Z}_{Pr}\boldsymbol{q}_P + \boldsymbol{Z}_{sr}\boldsymbol{q}_{se}$.

3. Method

In this study a thin, rigid, and infinite barrier with a height of $H_b = 2.5$ m is considered between a primary source and the target zone where it is intended to reduce the noise (Figure 2). The barrier is considered sufficiently massy to avoid noise transmission through it. The barrier zone is a parallelepipedic volume within 0.5 m of the barrier's surfaces. This zone contains 341 candidate positions for the location of transducers. The candidate positions are distributed evenly with the space of 0.1 m in the X- and Z-directions. The grid in Figure 2 shows the candidate positions.

The noise source is located at (−7, 0, 0.3) m, with a power output of 1 W at each frequency and the frequency spectra formed by the center frequency of third of the octave band from 63 Hz to 1 kHz. The target zone is an area of size 10×8 m^2 at a height of 1.65 m which is covered with 15 receiver points. These points are used to calculate the

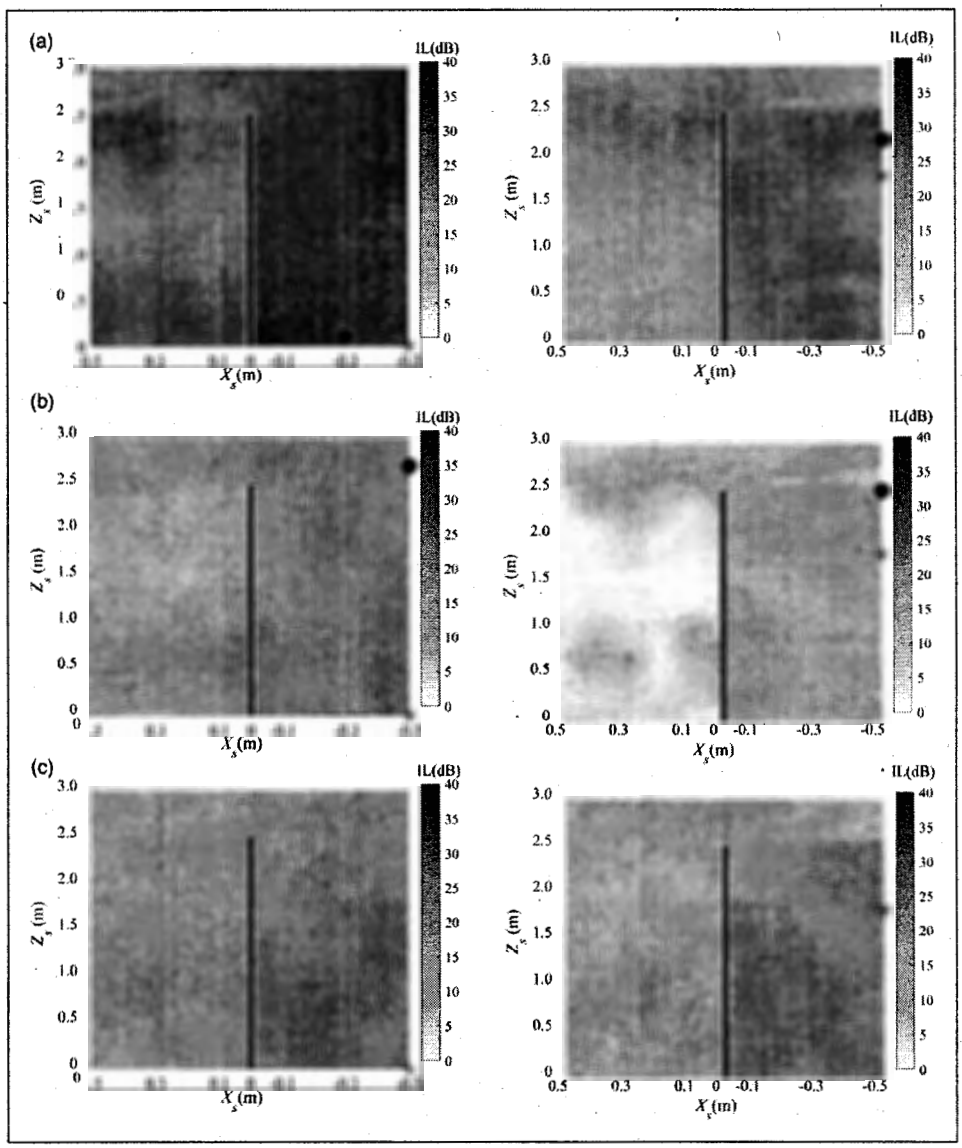

Figure 3. $\overline{IL}_r$ (dB) of all candidate positions of the control sources. (i) absorbent soil, (ii) hard soil. The barrier is represented by a black bar in the middle and ● represents the best position of the control sources. (a) 125 Hz, (b) 500 Hz, (c) overall, and * is the overall position of the control sources.

average insertion loss at the target zone according to Equations (9) and (10).

In the present work, ten control sources with interval space of $d_s = 0.2$ m are arranged linearly along the *Y*-direction and distributed symmetrically with respect to the *X*-axis. The distance between control sources is close to half of the shortest wavelength at 1 kHz which based on prior investigations (Elliott et al., 2018; Shao et al., 1997) ensures the best performance of an active control system. According to the number of receiver points and control sources, the quantities of $\boldsymbol{Z}_{Pr}$, $\boldsymbol{Z}_{sr}$, and $\boldsymbol{q}_{sr}$ in equation (6) are [15 × 1], [15 × 10], and [10 × 1], respectively.

Also, 41 error microphones with the same interval as the control sources $d_e = d_s = 0.2$ m are arranged linearly along the *Y*-direction and symmetrically with respect to the *X*-axis. The quantity of error microphones is $N_e = 41$ to cover the width of the target zone in the *Y*-direction. Thus, in equation (11), $\boldsymbol{Z}_{Pe}$, $\boldsymbol{Z}_{se}$, and $\boldsymbol{q}_{se}$ are vectors of size [41 × 1], [41 × 10], and [10 × 1], respectively.

To find the best location of control sources at each frequency, the insertion loss $\overline{IL}_r$ is computed for all candidate positions and the best one is selected. Afterward, the attenuation at the target zone is attempted by using a set of error microphones. To this end, the control sources are fixed

Table 2. $\overline{IL}_r$ (dB) at the best positions of error microphones with secondary sources at the positions in Table 1.

Absorbent soil				Hard soil		
Freq.(Hz)	(X_e, Z_e) m	$\overline{IL}_r$ (dB)	$\overline{IL}_{passive}$	(X_e, Z_e) m	$\overline{IL}_r$ (dB)	$\overline{IL}_{passive}$
63	(0.5, 1.5)	5.9	7.7	(0.5, 2.7)	14.9	8.4
80	(0.5, 1.2)	15.3	8.3	(0.5, 0.8)	9.7	9.4
100	(0.5, 1.9)	13.9	8.9	(0.2, 0.9)	13.6	8.9
125	(0.5, 2.1)	14.1	9.6	(0.5, 0.4)	18.8	8.4
160	(0.5, 2.2)	13.5	10.4	(0.5, 0.1)	15.4	9.8
200	(0.5, 2.1)	13.3	11.1	(0.5, 0.4)	8.2	15.2
250	(0.5, 2.3)	12.6	11.9	(0.4, 2.0)	7.1	12.1
315	(0.5, 2.2)	11.9	12.7	(0.1, 2.5)	2.5	12.5
400	(0.5, 2.2)	9.0	13.6	(0.3, 0.2)	4.8	14.6
500	(0.5, 0.5)	2.7	14.4	(0.5, 0.7)	4.5	20.0
630	(0.1, 0)	3.6	15.4	(0.5, 1.8)	3.4	21.6
800	(0.5, 2.4)	3.3	16.4	(0.2, 2.8)	1.6	34.1
1000	(0.4, 2.5)	2.5	17.4	(0.2, 2.5)	3.8	24.1
Overall	(0.5, 2.0)	(IL_o) 9.1	11.0	(0.4, 0.2)	(IL_o) 9.3	11.4

at the best position of each frequency and $\overline{IL}_r$ is calculated for all candidate positions of error microphones. Finally, the best position for the error microphones is where it gives the maximum reduction in the target zone. This two-step approach is repeated for the overall spectra to define the appropriate configuration of the broadband frequency range.

4. Results

4.1. Location of the secondary sources

Table 1 represents the best locations of the control sources together with the extra insertion loss achieved by active control means for both tonal noise $\overline{IL}_r$ and the overall frequency range IL_o. Furthermore, this table reports the reductions obtained by the passive barrier $\overline{IL}_{passive}$ at each frequency. This reduction defines the changes in the average pressure level at receivers after and before placing the barrier.

Those positions in Table 1 are the best locations for the array of control sources at each frequency and overall spectra. However, there are probably more suitable locations that get comparable attenuations in the shadow zone. In order to find these locations, Figure 3 represents the average insertion loss at the receivers $\overline{IL}_r$ for all 341 candidate positions at 125 Hz, 500 Hz, and the overall frequency range.

4.2 Location of the error microphones

Table 2 defines the best locations for error microphones among all 341 candidate positions when the control sources are located at the positions presented in Table 1. The error microphones at these positions achieve the maximum attenuation at the shadow zone.

Similar to Figure 3, Figure 4 shows the $\overline{IL}_r$ at the target zone while the error microphones are located in all 341 candidate positions, and control sources are placed in the best positions given in Table 1.

5. Discussion

5.1. Location of the secondary sources

Table 1 separately shows the noise level reduction of the passive barrier and the extra attenuation achieved with the active noise control system at the receivers. The total noise level reduction of the active noise barrier is the summation of these two noise control strategies. This table shows that the passive barrier operates more efficiently at high frequencies than low frequencies. However, the active noise control strategy compensates for the weak performance of the passive control at low frequencies.

Table 1 also shows the dependence of the exact best positions for the control sources and corresponding $\overline{IL}_r$ to the frequency and the soil reflection. Generally speaking, the best positions are at the incident side of the barrier and the active attenuation diminishes as the frequency increases, which are in complete agreement with all previous studies. Also, the negative effect of the soil reflections on the performance of the active noise barrier is presented. This is probably due to the more complex sound fields generated by the ground reflections on both sides of the barrier (Duhamel et al., 1998; Guo and Pan, 1998).

A more general trend can be found observing Figure 3 when the control sources are located at other candidate

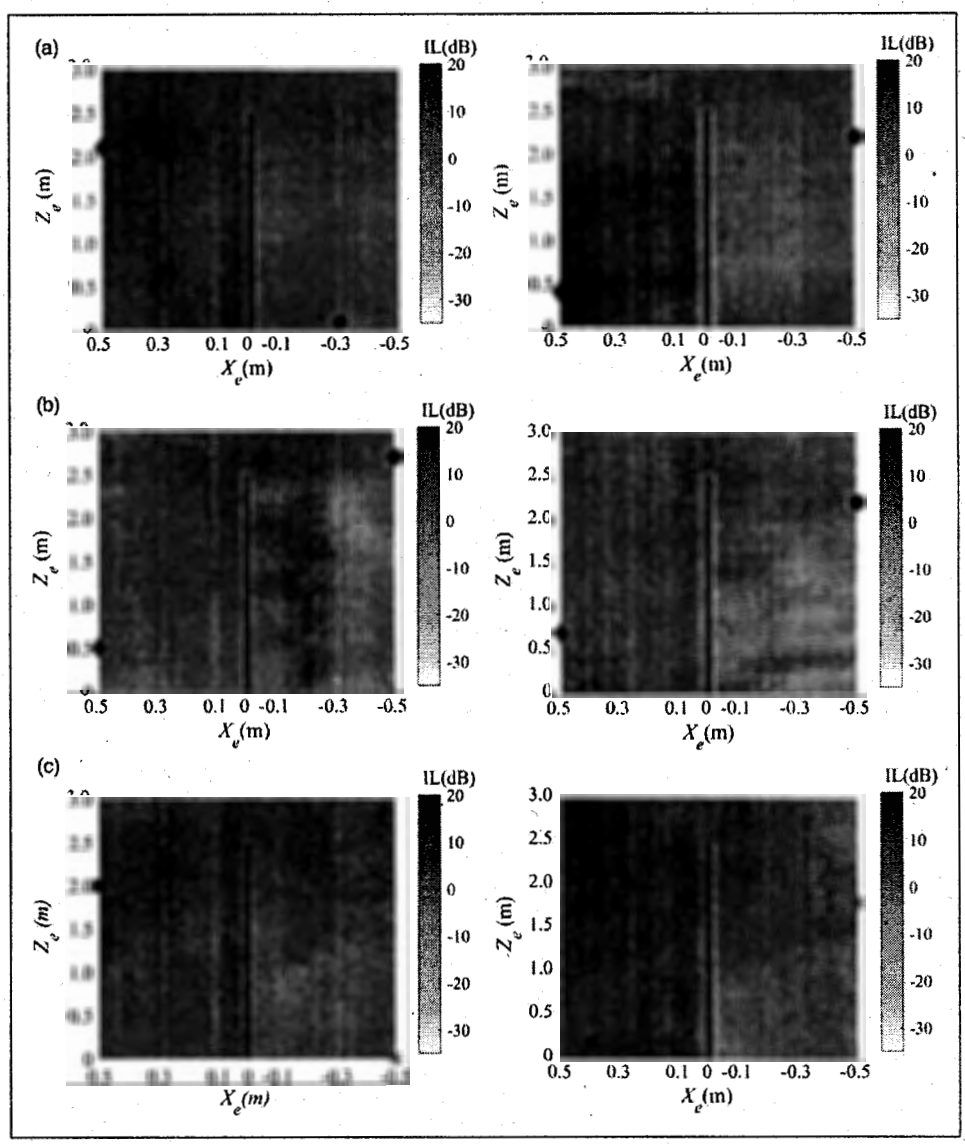

Figure 4. $\overline{IL}_r$ (dB) of all candidate positions of the error microphones in the barrier zone, (i) absorbent soil, (ii) hard soil. (a) 125 Hz, (b) 500 Hz, (c) overall. ● is the position of control sources at each frequency, ♦ is the best position of error microphones, * is the overall position of control sources, and ■ is the overall position of error microphones.

positions. Besides the suitable positions presented in Table 1, Figure 3 illustrates that there is a wide region of candidate positions where the control sources can obtain comparable results to the best position. Thus, it is possible to change the position of the control sources without losing significant performance, which is a general result consistent with previous observations (Duhamel et al., 1998; Han and Qiu, 2007; Hart and Lau, 2012). This observation is more obvious in the case of completely hard soil than absorbent soil.

Furthermore, Figure 3-ii illustrates that most of the incident region is suitable for placing the secondary source,

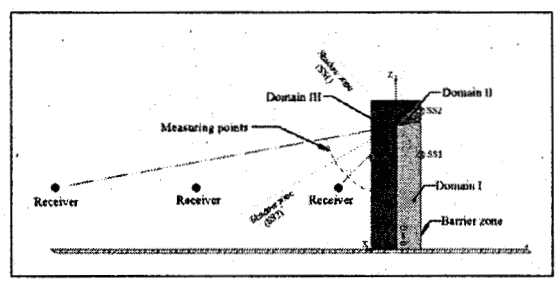

Figure 5. Schematic diagram of measuring points and three different domains for the control sources close to the barrier.

except a small domain at a height more than the barrier's tall. The secondary sources at this domain can only see part of the receivers. Taking this relation into account, it seems advisable to divide the barrier zone into three different domains. Domain I is at the incident side and below the path that connects the furthest receiver to the edge of the barrier. This domain includes those locations of control sources where all of the receivers are under the purely diffracted field of control sources, shown in Figure 5. The second domain (Domain II) is where some receivers can see the control sources (under the direct and diffracted fields) but the other receivers are located only in the diffracted field of control sources. Finally, Domain III represents those locations for control sources where "all" of the receivers are under the direct and diffracted control fields.

Locating the control sources in Domain II, the receivers are exposed to a mixture of direct and diffracted fields from the control sources. This mixture of different acoustic fields in the target zone seems to significantly lower the efficiency of active noise control. In order to find out whether this is the case, a phase analysis is performed. To this end, the phase of the primary and secondary fields are measured at several measuring points when the control sources are placed at each of those three domains. The measuring points shown in Figure 5 are located 1 m far from the edge and on a plane orthogonal to the barrier and centered at the edge of the barrier (Chen et al., 2013). The measuring points are in the angle range between 274° and 293°, which cover the direction from the edge of the barrier to all receivers. The control sources are located at SS1, SS2, and SS3 with coordinates of $(SS_x,SS_z) = (-0.5, 2.2)$, $(SS_x,SS_z) = (-0.5, 2.7)$, and $(SS_x,SS_z) = (+0.5, 2.0)$, respectively.

Figure 6 denotes the phase of the primary field ($\varnothing_0$), secondary field ($\varnothing_{SS}$), and their difference ($\Delta\varnothing$) at the measuring points. This figure indicates that when the secondary sources are at SS1 (Figure 6(a)), the primary and secondary fields are almost out of phase, which causes a decrease in the sound level in the target zone. However, for the other locations of secondary sources, $\varnothing_0$ and $\varnothing_{SS}$ are almost in-phase, which degrades the efficiency of the control system.

From the previous studies (Chen et al., 2013), and Figure 6(a), it is perceived that active noise control performs better when $|\Delta\varnothing|$ are close to 180°. Figure 7(a) and

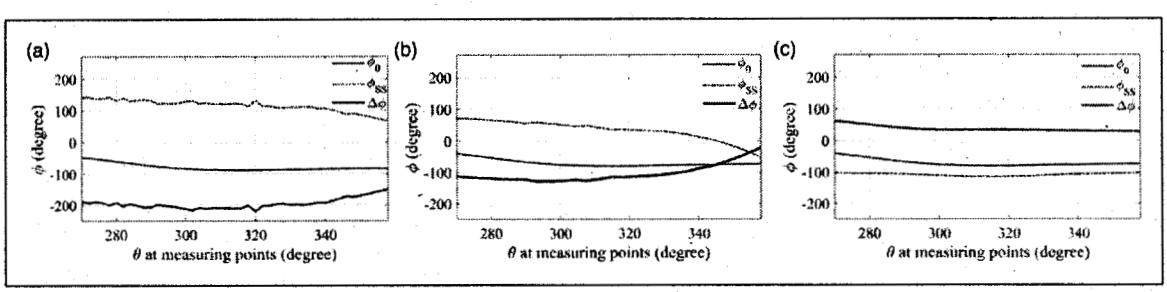

Figure 6. Phase of the primary field ($\varnothing_0$) and secondary field ($\varnothing_{SS}$) and their difference $\Delta\varnothing$ at measuring points 1 m from the top edge. Secondary sources are located at (a) SS1 ($SS_x = -0.5$, $SS_z = 2.2$), (b) SS2 ($SS_x = -0.5$, $SS_z = 2.7$), (c) SS3 ($SS_x = 0.5$, $SS_z = 2.0$). f = 125 Hz and hard soil.

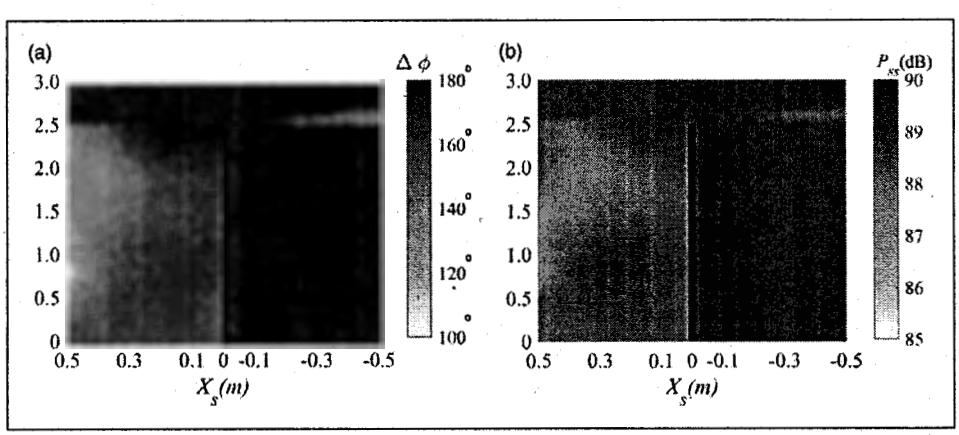

Figure 7. (a) The difference between the averaged phase of the primary and secondary field at receivers ($|\Delta\varnothing|$), (b) $\overline{IL}_r$, for different locations of secondary sources in the barrier zone f = 200 Hz and hard soil.

Figure 7(b) demonstrate $|\Delta\varnothing|$ and $\overline{IL}_r$ at all candidate positions. The comparison of these figures straightforwardly shows a high correlation between $|\Delta\varnothing|$ and $\overline{IL}_r$. This figure confirms that the active noise control performs more efficiently at those positions of secondary sources where $|\Delta\varnothing|$ are closer to the 180°, that is, the primary and control fields are out of phase.

As a conclusion of the analysis performed in Figure 6 and Figure 7, the higher attenuations achieved at the shadow zone when the diffracted field of the noise source is canceled by the control sources' diffracted fields. This general result is also supported by previous observations (Fan et al., 2013; Han and Qiu, 2007; Hart and Lau, 2012; Liuchun and Niu, 2008). Therefore, the proper locations of the control sources are in Domain I, where the primary diffracted field is controlled by a purely secondary diffracted field. Although for some frequencies, Table 1 shows that the best position for the secondary source is out of this domain, it is worth noting that these positions are rather isolated and cannot be used as general criteria. The use of these general criteria leads to a more robust configuration of the active noise barrier, because the small changes in locating the bulky secondary sources would result in the same attenuations as achieved at the best positions.

Previous findings are reinforced even when considering broadband spectra. For the broadband spectra, an entirely different calculation is performed to define the new suitable positions of control sources. For this purpose, equation (10) is used to calculate the overall insertion loss of the whole frequency spectra. As shown in Figure 3 (c), the overall insertion loss of the whole spectra is less depending on the position of the control sources than the single frequencies. Moreover, attenuation is achieved at any suitable position of the secondary sources, although the best zone is again in Domain I, as far as possible from the barrier.

Table 3. $\overline{IL}_r$ with the modified positions of control sources and error microphones.

Freq. (Hz)	Soil type	(X_s, Z_s) m	(X_e, Z_e) m	$\overline{IL}_r$ (dB)
63	Absorbent	(−0.5, 0)	(0.5, 2.4)	15.5
80	Hard	(−0.5, 1.8)	(0.5, 1.6)	12.5
315	Hard	(−0.5,1.8)	(0.3, 0.2)	8.0

5.2. Location of the error microphones

Table 2 shows in general terms the efficiency of the active noise barrier diminishes when attempting to reduce the primary field at error microphones out of the target zone, which is a rather expected result. Attenuation also decays with the increase of frequency, but with a trend that is not as smooth as for the secondary sources, since there is a dip in attenuation for those frequencies where the control sources are out of Domain I, that is, where the general criteria for the location of secondary sources are violated. (More notable in Table 2 at $f = 63$ Hz of absorbent soil, and $f = 80$ Hz and $f = 315$ Hz of hard soil).

Moreover, Table 2 shows that the proper locations of error microphones are mostly at the shadow side of the barrier, although these positions change by frequency. Similar to the previous step in order to define a suitable region for the error microphones, Figure 4 displays the $\overline{IL}_r$ for all candidate positions of the error microphones in the barrier zone. This figure shows that the best positions presented in Table 2 are not unique points, but there is a region in the barrier zone where the error microphones can locate without any significant loss of attenuation.

The results of Table 2 definitively suggest that for those frequencies which control sources located outside of Domain I, the performance of active control system with error microphones in the barrier zone reduce significantly. By modifying those positions of the control sources and locating them in Domain I, for instance, at the best position of

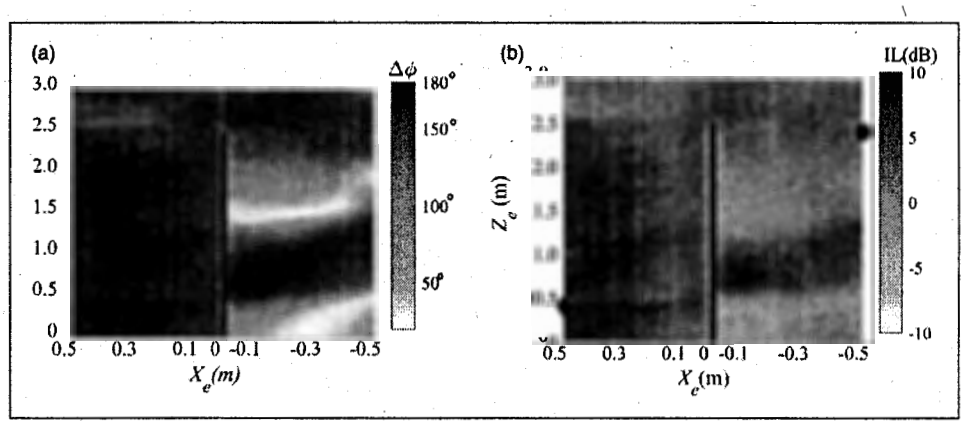

Figure 8. (a) Difference between the average phase of the primary and secondary field at receivers ($\Delta\varnothing$), and (b): $\overline{IL}$ (dB), for different locations of error microphones when the secondary sources are at $SS_x = -0.2$, $SS_z = 2.4$.

the broadband noise, and repeating the second step, greater attenuations at those frequencies are achieved. The results are presented in Table 3. These results are in a better correlation with those presented in Table 2 for other frequencies.

Generally speaking, as long as the control sources are in Domain I, the suitable region for the location of error microphones is on the shadow side and below the barrier edge. This trend simply suggests that the error microphones must be placed at any position so that they are under the diffracted fields of primary and secondary sources. In order to prove that hypothesis, the averaged phase difference at the receivers ($\Delta\varnothing$) is calculated at all of the candidate positions for error microphones, and the results are compared to the $\overline{IL}_r$ for the same configuration. Figure 8 compares $|\Delta\varnothing|$ with the $\overline{IL}_r$ at 200 Hz when the secondary sources are in the best position according to Table 1 ($SS_x = -0.5$, $SS_z = 2.4$). The comparison of Figure 8(a) and Figure 8(b) clearly shows that when the error microphones are located in the shadow zone of the barrier and the secondary sources are located in Domain I, the pressures of the primary and control sources are out of phase, which improves the performance of the active control system.

Consequently, the result shown in Figure 8 proposes that the active noise barrier operates more efficiently when the error microphones are located in the same acoustic field of all sources as the target zone is placed.

6. Conclusions

In this study, the cancellation mechanism of different placements of control units close to an active noise barrier is investigated to improve its performance. The active control system has a greater efficiency when the primary field is attenuated by interference with the control fields instead of suppressing the diffracted field at the barrier's edge as many of previous works attempted. Thus, the amplitude of the diffracted control field must be similar to the diffracted primary field. To achieve such control fields, general criteria for the placement of transducers are established. Based on that, the control sources must be placed on the incident side and below the path that connects the furthest receiver to the edge of the barrier and the error microphones should be located at the receiver side but in the shadow zone of both primary and control sources. It is shown that probably there are positions for control sources out of the optimal region that achieves good attenuation in the first step; however, when the control sources are coupled to a set of error sensors instead of the receivers, those positions give poorer reductions.

Furthermore, it is shown that the soil's reflection destructively affects the performance of the active control system in the narrowband cancellation. Despite this significant effect, the general criteria are valid for both the reflective and the absorptive soils. Also, it is noted that the two-step approach is suitable for the design of a compact active noise barrier whose cancelation zone is far away from the shadow zone, although it probably fails to find the absolute best configuration if the general criteria are ignored.

Acknowledgments

S. Sohrabi. would like to express his gratitude to the Agència de Gestió d'Ajuts Universitaris i de Recerca (AGAUR) (2020 FI_B2 00073) for the financial support.

Declaration of conflicting interests

The author(s) declared no potential conflicts of interest with respect to the research, authorship, and/or publication of this article.

Funding

The author(s) received no financial support for the research, authorship, and/or publication of this article.

ORCID iD

Shahin Sohrabi https://orcid.org/0000-0001-7148-4418

References

Aggogeri F, Merlo A and Pellegrini N (2020) Active vibration control development in ultra-precision machining. In: *Journal of Vibration and Control*. London, England: SAGE Publications Sage UK. ISBN 1077546320933477.

Ai Y, Qiu X and Hansen CH (2000) Minimizing wind effects on active control systems for attenuating outdoor transformer noise. *Noise Control Engineering Journal* 48: 130. DOI: 10.3397/1.2827968.

Aslan F and Paurobally R (2018) Modelling and simulation of active noise control in a small room. *Journal of Vibration and Control* 24(3): 607–618. SAGE Publications Sage UK, London, England

Attenborough K (1988) Review of ground effects on outdoor sound propagation from continuous broadband sources. *Applied Acoustics* 24(4): 289–319. DOI: 10.1016/0003-682X(88)90086-2.

Berkhoff AP (2005) Control strategies for active noise barriers using near-field error sensing. *The Journal of the Acoustical Society of America* 118(3): 1469–1479. DOI: 10.1121/1.1992787.

Borchi F, Carfagni M, Martelli L, et al. (2016) Design and experimental tests of active control barriers for low-frequency stationary noise reduction in urban outdoor environment. *Applied Acoustics* 114: 125–135. Elsevier Ltd. DOI: 10.1016/j.apacoust.2016.07.020.

Chen W, Min H and Qiu X (2013) Noise reduction mechanisms of active noise barriers. *Noise Control Engineering Journal* 61(2): 120–126. DOI: 10.3397/1.3702011.

Duhamel D, Sergent P, Hua C, et al. (1998) Measurement of active control efficiency around noise barriers. 55(3).

Elliott SJ, Cheer J, Bhan L, et al. (2018) A wavenumber approach to analysing the active control of plane waves with arrays of

secondary sources. *Journal of Sound and Vibration* 419: 405–419, Elsevier Ltd. DOI: 10.1016/j.jsv.2018.01.028.

Embleton TFW (1996) Tutorial on sound propagation outdoors. *The Journal of the Acoustical Society of America* ■■■: ■■■. DOI: 10.1121/1.415879.

Fan R, Su Z and Cheng L (2013) Modeling, analysis, and validation of an active T-shaped noise barrier. *The Journal of the Acoustical Society of America* 134(3): 1990–2003. DOI: 10.1121/1.4817887.

Guo J and Pan J (1998) Increasing the insertion loss of noise barriers using an active-control system. *The Journal of the Acoustical Society of America* 104(6): 3408–3416. DOI: 10.1121/1.423924.

Guo J, Pan J and Bao C (1997) Actively created quiet zones by multiple control sources in free space. *The Journal of the Acoustical Society of America* 101(3): 1492–1501. DOI: 10.1121/1.420362.

Han N and Qiu X (2007) A study of sound intensity control for active noise barriers. *Applied Acoustics* 68(10): 1297–1306. DOI: 10.1016/j.apacoust.2006.07.002.

Hart CR and Lau S-K (2012) Active noise control with linear control source and sensor arrays for a noise barrier. *Journal of Sound and VibrationElsevier* 331(1): 15–26. DOI: 10.1016/j.jsv.2011.08.016.

Huang X, Zou H and Qiu X (2015) A preliminary study on the performance of indoor active noise barriers based on 2D simulations*Building and Environment* 94: 891–899. Elsevier Ltd. DOI: 10.1016/j.buildenv.2015.06.034.

Lee HM, Wang Z, Lim KM, et al. (2019) A review of active noise control applications on noise barrier in three-dimensional/open space: myths and challenges. *Fluctuation and Noise Letters* 18(4): 1930002–1930021. DOI: 10.1142/S0219477519300027.

Li KM and Wong HY (2005) A review of commonly used analytical and empirical formulae for predicting sound diffracted by a thin screen. *Applied Acoustics* 66(1): 45–76. DOI: 10.1016/j.apacoust.2004.06.004.

Liuchun JC-C and Niu F (2008) Study on the analogy feedback active soft edge noise barrier. *Applied Acoustics* 69(8): 728–732. DOI: 10.1016/j.apacoust.2007.02.008.

Matsui T, Takagi K, Hiramatsu K, et al. (1989) Outdoor sound propagation from a source having dimensions. *The Journal of the Acoustical Society of Japan* ■■■: ■■■. DOI: 10.20697/jasj.45.7_512.

Nagamatsu H, Ise S and Shikano K (2000) Optimum arrangement of secondary sources and error sensors for active noise barrier. 1(August): 2–6.

Nelson PA, Elliott SJ and Stephen J (1992) *Active Control of Sound*. London: Academic.

Niu F, Zou H, Qiu X, et al. (2007) Error sensor location optimization for active soft edge noise barrier. *Journal of Sound and Vibration* 299(1–2): 409–417. DOI: 10.1016/j.jsv.2006.08.005.

Omoto A, Takashima K, Fujiwara K, et al. (1997) Active suppression of sound diffracted by a barrier: an outdoor experiment. *The Journal of the Acoustical Society of America* 102(3): 1671–1679. DOI: 10.1121/1.420078.

Palacios JI, Romeu J and Balastegui A (2010) Two step optimization of transducer locations in single input single output tonal global active noise control in enclosuresjournal of vibration and acoustics. *Journal of Vibration and Acoustics* 132(6): 061011. DOI: 10.1115/1.4002122.

Qiu X, Qin M and Zou H (2017) Active control of sound transmission through a hole in a large thick wall. In: Proceedings of ACOUSTICS 2017 Perth: Sound, Science and Society - 2017 Annual Conference of the Australian Acoustical Society AAS, 2017(1), Australia, ■■■, pp. 1–8.

Romeu J., Palacios JI, Balastegui A, et al. (2015) Optimization of the active control of turboprop cabin noise. *Journal of AircraftAmerican Institute of Aeronautics and Astronautics* 52(5): I386–1393. DOI: 10.2514/1.C032431.

Shao J, Sha J-Z and Zhang Z-L (1997) The method of the minimum sum of squared acoustic pressures in an actively controlled noise barrier. *Journal of Sound and Vibration* 204(2): 381–385. DOI: 10.1006/jsvi.1997.0909.

Sohrabi S, Pàmies Gómez T and Romeu Garbí J (2020) Suitability of active noise barriers for construction sites. *Applied Sciences* 10(18): 6160. DOI: 10.3390/app10186160.

Wang X, Koba Y, Ishikawa S, et al. (2016) Hybrid actice noise barrier with sound masking in open-plan offices. *Noise Control Engineering Journal* 64(3): 403–415. DOI: 10.3397/1/376389.